Monthly Notices of the ROYAL ASTRONOMICAL SOCIETY

MNRAS **462,** S562–S572 (2016) doi:10.1093/mnras/stw3370
Advance Access publication 2017 January 7

First *in situ* detection of the cometary ammonium ion NH_4^+ (protonated ammonia NH_3) in the coma of 67P/C-G near perihelion

A. Beth,[1⋆] K. Altwegg,[2] H. Balsiger,[2] J.-J. Berthelier,[3] U. Calmonte,[2] M. R. Combi,[4] J. De Keyser,[5] F. Dhooghe,[5] B. Fiethe,[6] S. A. Fuselier,[7,8] M. Galand,[1] S. Gasc,[2] T. I. Gombosi,[4] K. C. Hansen,[4] M. Hässig,[2,7] K. L. Héritier,[1] E. Kopp,[2] L. Le Roy,[2] K. E. Mandt,[7,8] S. Peroy,[1] M. Rubin,[2] T. Sémon,[2] C.-Y. Tzou[2] and E. Vigren[9]

[1]*Department of Physics, Imperial College London, Prince Consort Road, London SW7 2AZ, UK*
[2]*Physikalisches Institut, University of Bern, CH-3012 Bern, Switzerland*
[3]*LATMOS/IPSL-CNRS-UPMC-UVSQ, 4 Avenue de Neptune, F-94100 Saint-Maur, France*
[4]*Department of Atmospheric, Oceanic and Space Sciences, University of Michigan, 2455 Hayward, Ann Arbor, MI 48109, USA*
[5]*BIRA-IASB, Royal Belgian Institute for Space Aeronomy, Ringlaan 3, B-1180 Brussels, Belgium*
[6]*Institute of Computer and Network Engineering (IDA), TU Braunschweig, Hans-Sommer-Straße 66, D-38106 Braunschweig, Germany*
[7]*Department of Physics and Astronomy, University of Texas at San Antonio, San Antonio, TX 78228-0510, USA*
[8]*Southwest Research Institute San Antonio, San Antonio, TX 78228, USA*
[9]*Swedish Institute of Space Physics, SE-75121 Uppsala, Sweden*

Accepted 2016 December 23. Received 2016 November 23; in original form 2016 June 29

ABSTRACT

In this paper, we report the first *in situ* detection of the ammonium ion NH_4^+ at 67P/Churyumov–Gerasimenko (67P/C-G) in a cometary coma, using the Rosetta Orbiter Spectrometer for Ion and Neutral Analysis (ROSINA)/Double Focusing Mass Spectrometer (DFMS). Unlike neutral and ion spectrometers onboard previous cometary missions, the ROSINA/DFMS spectrometer, when operated in ion mode, offers the capability to distinguish NH_4^+ from H_2O^+ in a cometary coma. We present here the ion data analysis of mass-to-charge ratios 18 and 19 at high spectral resolution and compare the results with an ionospheric model to put these results into context. The model confirms that the ammonium ion NH_4^+ is one of the most abundant ion species, as predicted, in the coma near perihelion.

Key words: astrochemistry – plasmas – methods: data analysis – Sun: UV radiation – comets: individual: 67P.

1 INTRODUCTION

On 2015 August 13, 67P/Churyumov–Gerasimenko (Churyumov & Gerasimenko 1972, hereafter referred as 67P/C-G), reached its perihelion at ∼1.24 au, a milestone for its cometary activity and the observations performed by the European Space Agency's *Rosetta* mission at that time. It was expected that the outgassing rate of 67P/C-G reached $Q = 4–8 \times 10^{27}$ molecules s^{-1} (Hanner et al. 1985; Benna & Mahaffy 2006; Hansen et al. 2007; Lamy et al. 2007; Tenishev, Combi & Davidsson 2008). For 2015 July/August period, the Rosetta Orbiter Spectrometer for Ion and Neutral Analysis (ROSINA)/Comet Pressure Sensor (COPS) detected maximum local outgassing rates between 2×10^{27} and 7×10^{28} molecules s^{-1} within the uncertainty on the velocity outflow (500–1000 m s^{-1}). During late 2015 July/early August, shortly before perihelion, in 2015 July, *Rosetta* was able to probe the neutral and ion composition of the coma near the nucleus at a cometocentric distance between 150 and 200 km using the Double Focusing Mass Spectrometer (DFMS) from the ROSINA instrument.

This increased activity can efficiently trigger the production of new ion species, such as NH_4^+ (from the protonation of NH_3). Ammonia is a minor neutral species, which was previously detected in the coma of other comets such as: 1P/Halley (Meier et al. 1994; Rubin et al. 2011), C/1995 O1 (Hale-Bopp, Bird et al. 1997), C/1996 B2 (Hyakutake, Palmer et al. 1996; Bockelee-Morvan 1997), C/2012 F6 (Lemmon, Paganini et al. 2014), 103P/Hartley 2 (Dello Russo et al. 2011; Mumma et al. 2011; Kawakita et al. 2013), 73P/SW3/B and 73P/SW3/C (Dello Russo et al. 2007), 6P/d'Arrest and 17P/Holmes (Dello Russo et al. 2009) and also at 67P/C-G (Le Roy et al. 2015). Even if the NH_3 mixing ratio is relatively small (i.e. less than 2 per cent relative to water), its presence plays a key role in the chemistry of the hydronium ion H_3O^+, found to be the dominant ion of 67P at a 30 km cometocentric distance for low activity at heliocentric distances ∼3 au (Fuselier et al. 2015). As H_2O has a lower proton affinity than NH_3, the proton transfer reaction from H_3O^+ to NH_3 is efficient producing NH_4^+. Ionospheric modelling studies that include the production of NH_4^+ have already

⋆ E-mail: arnaud.beth@gmail.com

been undertaken for comet 1P/Halley with a high outgassing rate (see Allen et al. 1987; Wegmann et al. 1987; Haider, Bhardwaj & Singhal 1993; Haider & Bhardwaj 2005; Rubin et al. 2009) and for 67P/C-G (Vigren & Galand 2013), inside the contact surface (Balsiger et al. 1986; Neubauer et al. 1986). The *in situ* detection of NH_4^+ is a challenge: its mass-to-charge ratio is 18.038 u/e, close to the water ion mass of 18.015 u/e and therefore requires high-mass resolution for separation of the two components.

At 1P/Halley, with the High Intensity Spectrometer (HIS) on-board Giotto, Balsiger et al. (1987) measured abundant cold ions associated with the water ion group (Balsiger et al. 1986; Altwegg et al. 1993) but its spectral resolution was not good enough to distinguish species with overlapping mass-to-charge ratios, mostly between 14 and 18 u/e (e.g. H_2O^+ and NH_4^+, see Allen et al. 1987; Altwegg et al. 1993). However, for 67P/C-G, with the ROSINA/DFMS (Balsiger et al. 2007) on board, the high spectral resolution effectively separates species for similar *m/q*. In that context, Vigren & Galand (2013) predicted: (1) the presence of NH_4^+; (2) other ions associated with neutrals having higher proton affinity than water and their dominance over H_3O^+ within the diamagnetic cavity near perihelion.

In this paper, we present the first *in situ* detection of NH_4^+ ions from a comet, using the mass spectrometer DFMS on-board *Rosetta*. To put these observations into context, the observed ion composition is compared with the simulations from our ionospheric model (updated from Vigren & Galand 2013) applied to the observed conditions encountered in the coma of 67P/C-G near perihelion. In Section 2, we present a summary of the procedure applied for the data analysis of DFMS, while, in Section 3, the ionospheric model and the chemistry of NH_4^+ are described. We present the observational results from 2015 July 29 to August 1 in Section 4 and a comparison with the model in Section 5. Finally, a discussions is given in Section 6 and conclusions are presented in Section 7.

2 DATA ANALYSIS

DFMS is a double focusing magnetic mass spectrometer, type Mattauch-Herzog, with a mass range 12–150 u. It is optimized for very high-mass resolution (a mass resolution of 3000 at 1 per cent peak height) and large dynamic range (Balsiger et al. 2007). In this section, we summarize the list of procedures for the analysis of the ion mode data.

After ions enter the DFMS instrument, they are accelerated by a mass-dependent acceleration voltage, then deflected by an electrostatic analyser and by a magnetic field (selection according to their mass-to-charge ratio) and finally hit the Multi-Channel Plate (MCP)/Linear Electron Detector Array (LEDA). The LEDA is divided into two rows/channels, A and B (Balsiger et al. 2007). The detector delivers a signal that needs to be converted into physical units, the number of ions per second (or per spectrum).

Several steps are needed for calibrating the ion raw data of ROSINA/DFMS in ion mode. First, the offset of the MCP/LEDA has to be removed: this offset is approximated by a third-order polynomial. Only MCP pixels without any peaks are used to determine this polynomial.

Secondly, the gain of each pixel is different and decreases with time due to the ageing of the MCP. The gain for each pixel is a function of the Gain Step (GS): this determines a global gain for all pixels (e.g. a constant gain to apply to all pixels) and the gain of an individual pixel. In particular, the gain for central pixels is lower: this gain depends on the number of ions that impacted on a pixel during the instrument's history. H_2O^+ and H_3O^+ impact in the middle of the pixel range. This should be carefully corrected: the gain was 60 per cent less than the maximum in 2014. A detailed procedure is provided by Le Roy et al. (2015, regarding the conversion from counts to intensity in number of ions per spectrum or second).

Regarding mass calibration, the conversion of the pixel position x, an integer between 1 and 512, on the LEDA detector into an ion mass (m/q) is given by

$$M(p) = M_0 \exp\left(\frac{x(p-p_0)}{Dz}\right), \quad (1)$$

where M_0 is the commanded mass-to-charge ratio ($m/q = 18$ u/e for H_2O^+ and NH_4^+, $m/q = 19$ u/e for H_3O^+), p_0 is the pixel position for the mass m_0, x is the centre-to-centre distance between adjacent pixels ($x = 25$ μm), D is the dispersion constant (1.23×10^5 μm) and z is a zoom factor depending on the mode: 1 for low resolution (LR) and ∼6.4 for high resolution (HR). p_0 may vary depending on the temperature of the magnet and the commanded mass-to-charge ratio. For $M_0/q = 18$ or 19 u/e, p_0 is expected to be located around 280 for the time interval investigated in this paper. As the term Dz is $\gg x(p-p_0)$, the separation by one pixel corresponds to a separation by $\Delta m/q = 3.6 \times 10^{-3}$ u/e for LR and $\Delta m/q = 5.6 \times 10^{-4}$ u/e for HR at $m/q \approx 18$–19 u/e. As mentioned by Balsiger et al. (2007), the mass resolution achieved by the instrument is $m/\Delta m = 5000$ in HR and $m/\Delta m = 800$ in LR, which means the LR mode is not able to separate H_2O^+ and NH_4^+ peaks ($\Delta m/q_{H_2O^+,NH_4^+} = 0.0238$ u/e).

On the one hand, the ion HR mode is not operated very often by ROSINA/DFMS. On the other hand, the mass-to-charge ratio $m/q = 18$ is the most scanned m/q by this mode: during each sequence of data acquisition, the mass 18 is scanned first and last for calibration and science purposes; meanwhile, data from $m/q = 13$ to 50 are acquired, during which $m/q = 18$ is scanned an additional time. Thus, for $m/q = 18$, there are three times as many measurements as for other masses.

Once ion data are calibrated (see Fig. 1), the line profile of each ion is assumed to be a Voigt distribution (VD), the convolution of a Lorentzian and a Gaussian distributions (see the Appendix). Other distributions could be used such as a pseudo-Voigt one (sum of one Lorentzian and one Gaussian) or two Gaussians, more appropriate of the neutral mode analysis for example (De Keyser et al. 2015). The VD has the advantage of a four parameter fit, as detailed in the Appendix. Due to the limited number of points to resolve one line profile (∼10), we have chosen the VD, which has the lowest number of fit parameters. However, the comparison between a double-Gaussian distribution and a VD showed residuals comparable to, and sometimes even better for the VD.

For each spectrum:

(i) We look for peaks near the expected location (±0.01 u/e to avoid contaminations by neighbouring peaks and/or a shift of x_0) for both channels. We assume a certain threshold for a good signal-to-noise ratio (SNR > 2–3, i.e. the peak count should be >3), to avoid a false positive and/or to have a sufficient amount of counts for a better fitting. The pixel p_0 and the peak position have to be considered carefully because equation (1) is approximate.

(ii) The peaks are fitted by four parameters: m_j the mass centre of the peak close to the ion mass, α the integrated area below the peak, σ and γ. Assuming a Voigt profile, the peak shape is approximated by $\alpha V(m - m_j, \sigma, \gamma)$, where V, σ and γ are defined in the Appendix.

(iii) The values are scaled by a factor allowing the conversion from the mass scale to the pixel scale: $\frac{dp}{dM} = \frac{Dz}{M(p)x} \approx \frac{32000}{M_0}$ according to equation (1). Here, the ion masses of interest are relatively

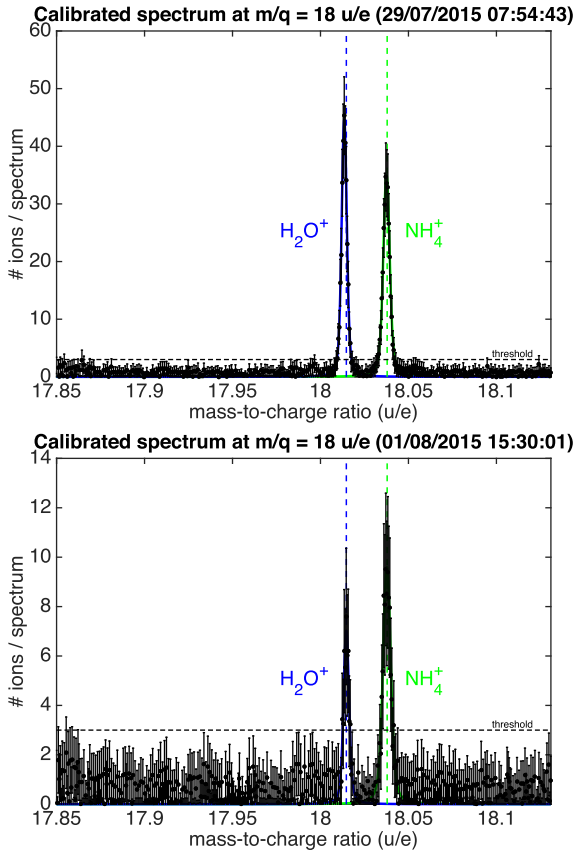

Figure 1. Example of HR spectra at mass 18. The abscissa is in unified atomic mass unit per charge. The data are represented by the black dots, the blue solid line corresponds to the fit by a VD for H_2O^+, the green one for NH_4^+. The coloured vertical dashed lines represent the expected locations of each ion and the horizontal one is the threshold that we assumed for a clean fitting.

close and the scaling factor is similar. For low counts, one could add both channels. However, if one of the channels is slightly more efficient than the other, then their pixels p_0 are different by $\gtrsim$2 pixels.

For the neutral mode, the number densities of individual species can be derived from the combination of DFMS (mixing ratios) and COPS (total density) data. For ions, DFMS alone cannot be used to derive ion densities because the small field of view and the limited energy acceptance ($9^\circ \times 6.5^\circ$ for ions at 5 eV, Schläppi 2011) limit the observed ions to a small fraction of the entire phase space.

Some uncertainties from different sources still remain:

(i) a statistical error ($\propto \sqrt{N_{\rm count}}$) as represented by the error bars ($\pm\sqrt{N_{\rm count}}$) on Fig. 1,
(ii) the precision on the gain of each pixel (~7 per cent),
(iii) the precision on the pixel p_0 depending on the mass and the temperature of the magnet,
(iv) the uncertainty on the pixel gain (~7 per cent) if all measurements are not performed with the same GS, which is not the case here.

For the fitting procedure, we assume that all data have the same weight to prevent high contribution from the noise.

3 MODEL

To help us to understand the ion observations, we use an updated version of the one-dimensional ionospheric model presented in Vigren & Galand (2013). The model solves the continuity equation for each ion:

$$\frac{\partial n_j}{\partial t} + \frac{1}{r^2}\frac{\partial}{\partial r}\left(n_j(r) r^2 U_j(r)\right) = P_j(r) - L_j(r) n_j(r), \quad (2)$$

where n_j is the density of ion species j, U_j its radial velocity, r the distance from the centre of the comet, P_j the production rate (associated with e.g. photoionization and ion–neutral reactions) and $L_j n_j$ the chemical loss rate (associated with e.g. ion–neutral reactions and electron–ion dissociative recombination) associated with the ion species j. The model is solved based on an explicit forward Euler method in time and position and assumes a constant radial outflow. The time step is adapted to be always one hundred times lower than any time-scales (production, loss, advection). The model is solved from 2 km (radius of the cometary nucleus) to 2000 km, with distances logarithmically spaced. The results presented in Section 4 correspond to the equilibrium i.e. all ion species reach the condition $\partial n_j/\partial t = 0$, when the advection term is balanced by local production and chemical losses.

We impose a constant neutral background, not influenced by the ion chemistry. Assuming a constant velocity and flux conservation, the number density $n_{\rm n}$ of a neutral species n is given by

$$n_{\rm n}(r) = \frac{Q_{\rm n}}{4\pi r^2 U_{\rm n}} = \frac{Q f_{\rm n}}{4\pi r^2 U_{\rm n}}, \quad (3)$$

where $Q_{\rm n}$ is the outgassing rate of the neutral species n, Q the total outgassing rate (i.e. $\sum_{\rm n} Q_{\rm n} = Q$) constrained by COPS for a given $U_{\rm n}$, $f_{\rm n}$ the volume mixing ratio of the species n (i.e. $\sum_{\rm n} f_{\rm n} = 1$), constrained by DFMS data and $U_{\rm n}$ the neutral outflow speed, in the range of 500–1000 m s^{-1}. This $1/r^2$ dependence is justified from observations (Bieler et al. 2015; Hässig et al. 2015). The exact velocity of ions is unknown and we assume that this is equal to the neutral velocity ($U_j(r) \approx U_{\rm n}$). For this study, we assume a mixture of pure water and ammonia. In addition, the neutral ($T_{\rm n}$), ion ($T_{\rm i}$) and electron ($T_{\rm e}$) temperatures are assumed to be all equal to 200 K. $T_{\rm n}$ and $T_{\rm i}$ influence ion–neutral reaction rates, while $T_{\rm e}$ is driving electron–ion dissociate recombination rates. The sensitivity of the ionospheric composition and densities as a function of temperatures is discussed in Section 6.1.

The simulations are also constrained with the near nucleus coma and therefore we can neglect terms associated with photoionization loss for the neutrals.

3.1 Photoionization of cometary neutrals

Because of the high activity of the comet near perihelion ($Q \sim 1 - 3 \times 10^{28}$ molecules s^{-1}, depending on *Rosetta* latitude relative to the subsolar one), the coma is optically thick to extreme ultraviolet solar radiation. Photoabsorption is taken into account for photoionization of H_2O and NH_3. As we assume a spherical symmetry and a $1/r^2$ law for the neutral densities, the column density, $N_{\rm n}$, of the species n (and thus its optical depth) at a given cometocentric distance r and solar zenith angle χ is given by

$$\begin{aligned} N_n(r,\chi) &= \int_{r\cos\chi}^{+\infty} n_{\rm n}(s)\,{\rm d}s \\ &= \int_{r\cos\chi}^{+\infty} \frac{Q_{\rm i}}{4\pi U_{\rm n}(s^2 + r^2\sin^2\chi)}\,{\rm d}s \\ &= \frac{Q_{\rm n}}{4\pi U_{\rm n} r}\frac{\chi}{\sin\chi} = n_{\rm n}(r) r \frac{\chi}{\sin\chi}, \end{aligned} \quad (4)$$

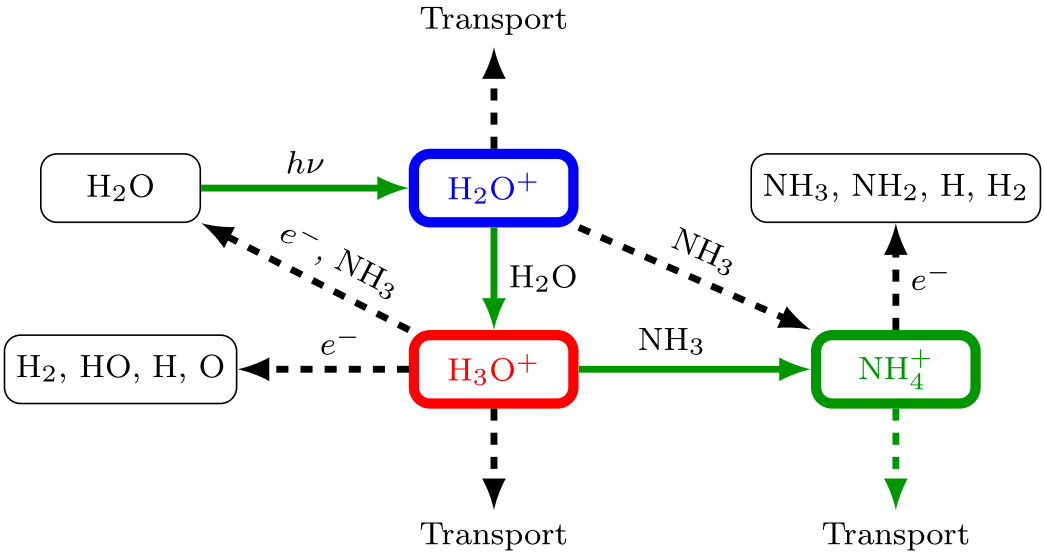

Figure 2. Most efficient pathway leading to the production of NH_4^+ (solid, green arrows) and its loss (dashed, green arrows). Black dashed arrows represent additional loss processes for the three key species, such as e^-–ion dissociative recombination, ion–neutral reactions or transport.

where s is the abscissa along the line of sight from the position (r, χ) towards the Sun.

As the solar zenith angle was close to 90° during 2015 July and August, the optical depth was consequently set to reproduce the conditions of observations: the column density and thus the optical depth in the terminator plane is $\pi/2 - 1 \approx 57$ per cent higher compared to along the Sun–comet axis for the same cometocentric distance. The solar irradiance considered is based on TIMED/SEE observations from the Earth on 2015 July 21 and extrapolated to the location of 67P/C-G.

3.2 Chemistry of ammonium ion: transfer of a proton from H_2O^+ to NH_4^+

The main role of NH_3 in the coma is assessed as a function of its density relative to water and the ion outflow velocity. The influence of other neutral coma species, such as CO and CO_2, were also assessed but they did not have a major impact on H_2O^+, H_3O^+ (Fuselier et al. 2016) and NH_4^+ chemistry.

For a mixture of water and ammonia, the main chemical pathways are illustrated in Fig. 2. The formation of NH_4^+ requires three reactions (one photoionization and two ion–neutral collisions) and results in the formation of two intermediate ions.

First, H_2O is ionized by solar radiation at the rate ν_{H_2O}, the photoionization frequency, which is a function of r as the coma is optically thick, producing H_2O^+:

$$H_2O + h\nu_{ion} \xrightarrow{\nu_{H_2O}} H_2O^+ + e^- \quad \nu_{H_2O}(\infty) = 2.22 \times 10^{-7} s^{-1}, \quad (5)$$

where $\nu_{H_2O}(\infty)$ is the non-attenuated photoionization rate at a heliocentric distance of ∼1.25 au and $h\nu_{ion}$ is the required energy for this process. Near perihelion, the largest production of H_2O^+ is due to closer proximity of the comet to the Sun and the maximum activity ($Q \sim 10^{28}$ molecules s^{-1}).

The newborn H_2O^+ then reacts readily with the surrounding dominant neutral species, H_2O:

$$H_2O + H_2O^+ \xrightarrow{k_1} H_3O^+ + HO \quad k_1(200\,K) = 2.57 \times 10^{-9} cm^3\, s^{-1}. \quad (6)$$

This reaction is a proton transfer: the proton affinity of H_2O (7.17 eV, Hunter & Lias 1998) is higher than the one of HO (6.16 eV, Hunter & Lias 1998). Indeed, the proton affinity refers to the ability for a neutral atom or molecule to capture a proton. Similar to acid/base reactions, the proton is preferentially transferred to the species with the highest proton affinity.

For strong cometary activity, time-scales for both reactions are significantly lower than the advection (defined by equation 12) time-scale (away from the surface) so that H_2O^+ is close to the photochemical equilibrium:

$$0 \approx \nu_{H_2O}(\infty) n_{H_2O}(r) - k_1 n_{H_2O}(r) n_{H_2O^+}(r), \quad (7)$$

where ν_{H_2O} is only valid in the optically thin part of the coma, a few hundred kilometres above the cometary surface. Equation (7) leads to

$$n_{H_2O^+}(r) \approx \frac{\nu_{H_2O}}{k_1} \approx 10^2\ cm^{-3}. \quad (8)$$

In the absence of species with higher proton affinities and/or sufficient cometary activity, H_3O^+ is the terminal ion that is only lost by transport (Fuselier et al. 2015) or dissociative ion–electron recombination in environments of extremely low electron temperature. However, during 2015 July and August, ROSINA/DFMS observed a proportion of NH_3 up to 0.5 per cent in agreement with Microwave Instrument on the Rosetta Orbiter observations (Biver et al. 2015). NH_3 has a proton affinity (8.86 eV, Hunter & Lias 1998), higher than the proton affinity of H_2O and thus may react through proton transfer with H_3O^+, the dominant ion in the collision dominated part of the coma:

$$NH_3 + H_3O^+ \rightarrow NH_4^+ + H_2O. \quad (9)$$

According to the relative amount of NH_3 with respect to H_2O, NH_4^+ might become the dominant ion in some part of the coma, especially close to the surface. Indeed, the production of NH_4^+ occurs mostly close to the surface, where NH_3 and H_3O^+ number densities are highest. However, H_3O^+ needs one less reaction to be produced such as it can be still dominating the ion composition.

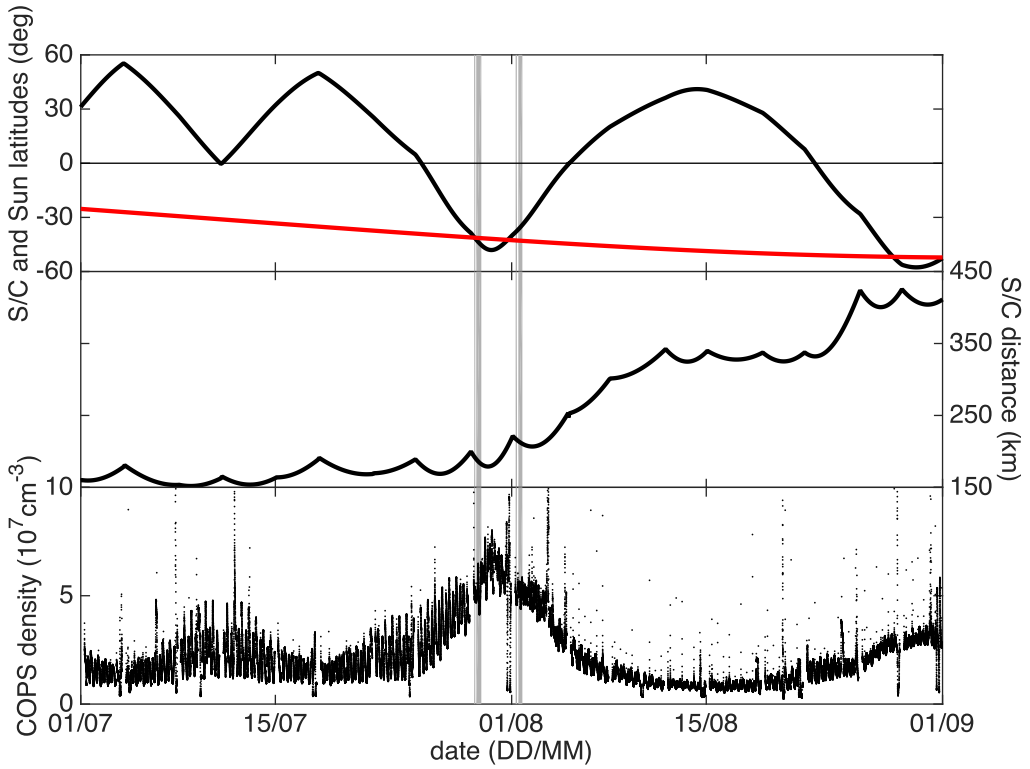

Figure 3. Conditions encountered in 2015 July and August. Upper panel: *Rosetta* (black) and Sun (red) latitudes in the rotating comet frame; middle panel: *Rosetta* distance from the comet; bottom panel: uncalibrated COPS density. The grey areas around August 1 correspond to the periods of observation for the case studies. COPS densities were affected by manoeuvres, altitude spacecraft changes and wheel offloading.

3.3 Other possible pathways

Other shorter chemical paths with less intermediary reactions also lead to the production of NH_4^+ but are significantly less efficient:

(i) NH_3 can react directly with H_2O^+:

$$NH_3 + H_2O^+ \rightarrow NH_4^+ + HO. \quad (10)$$

However, according to their respective densities (one or two orders of magnitude less than H_3O^+ for H_2O^+, see Fuselier et al. 2016; two orders of magnitude less than H_2O for NH_3), H_2O^+ preferentially reacts with H_2O, which caps its density, and NH_3 with H_3O^+.

(ii) NH_3 can be photoionized and readily reacts with H_2O:

$$\begin{cases} NH_3 + h\nu \rightarrow NH_3^+ + e^- \\ NH_3^+ + H_2O \rightarrow NH_4^+ + HO. \end{cases} \quad (11)$$

Although less efficient, these reactions have been included in our ionospheric model for completeness. For a more complete overview of the ion–neutral chemistry within the coma and with other minor species, we refer to Allen et al. (1987) for 1P/Halley.

4 CASE STUDIES

Past observations during 2014 October (Le Roy et al. 2015) revealed a relatively low volume mixing ratio of NH_3 with respect to H_2O in the coma compared with other comets: 0.06 per cent above the illuminated Northern hemisphere (summer at the time of the observations) and 0.15 per cent above the Southern hemisphere. These abundances should be compared with the value at 1P/Halley of about 1.5 per cent (Meier et al. 1994; Rubin et al. 2011). However, observations from DFMS near perihelion during 2015 July when the Southern hemisphere was in summer revealed an increase in the ammonia mixing ratio up to 0.5 per cent.

The chemistry and detection of NH_4^+ require high density/activity of the comet. We investigate the periods when COPS detected the highest neutral number densities near perihelion, on 2015 August 1. Indeed, several factors favouring high densities occurred simultaneously:

(i) *Rosetta* flew over latitudes similar to the subsolar latitude in the frame attached to the comet ($\sim -42^\circ$, see Fig. 3, top panel), which means that *Rosetta* was over regions which were subsolar and directly illuminated during the comet day, for a few hours ($\sim$3 h),

(ii) *Rosetta* was within 200 km from the comet ($\sim$200 km, see Fig. 3, middle panel),

(iii) 67P/C-G was near perihelion (2015 August 13) and its activity was close to its maximum. Also, photoionization rates were typically higher compared to the rest of the orbit.

The periods selected in this paper are associated with a substantial time of observations when NH_4^+ has been successfully detected: in HR ion mode from 2015 July 29 to August 1 (see Fig. 3, grey periods). No other observations in HR ion mode are available between these days.

NH_4^+ was also observed during the early phase of the mission (e.g. 2015 January) but this is proved not to be of cometary origin, as discussed in Section 4.1. We present the observations from July 29 in Section 4.2 to August 1 in Section 4.3.

4.1 2015 January: a 'false positive'

During 2015 January, the analysis revealed the presence of NH_4^+, although the outgassing rate Q was low, around $\sim 3 \times 10^{26}$ s^{-1}

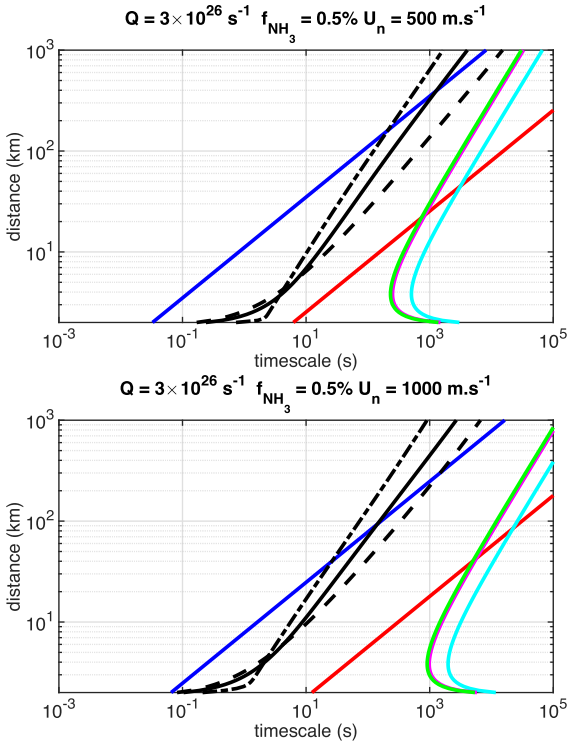

Figure 4. Loss time-scales for H_2O^+, H_3O^+ and NH_4^+ for $U_n = 500$ m s^{-1} (top panel) and 1000 m s^{-1} (bottom panel) for $Q = 3 \times 10^{26}$ s^{-1} and $f_{NH_3} = 0.5$ per cent, similar to 2015 January. The black lines correspond to the advection times of H_2O^+ (dot–dashed), H_3O^+ (solid) and NH_4^+ (dashed). The blue (respectively cyan) lines are the loss time-scales of H_3O^+ with NH_3 (respectively electrons). The green lines are the loss time-scales of NH_4^+ by recombination with electrons ($T_e = 200$ K).

($U_n = 1000$ m s^{-1}). However, its detection was correlated with spacecraft manoeuvres. Indeed, as mentioned by Schläppi et al. (2010), the gas cloud around the spacecraft may be contaminated by *Rosetta* itself. Amongst the contaminants of nitrogenated species, there is the propellant monomethylhydrazine. Other contaminants such as polyurethane, epoxies, polyamines – contained in structure, potting, etc. – are also common for spacecraft.

Another argument to reject the cometary origin of NH_4^+ for this period is the comparison of the loss time-scales for H_2O^+, H_3O^+ and NH_4^+ through chemistry and transport, as shown in Fig. 4. The time-scales refer to the characteristic times within the coma at a given cometocentric distance. Several time-scales can be defined, such as the chemical time-scale τ_{chem} and the advection time-scale τ_{adv}. The chemical time-scale is defined as: $\tau_{chem}(r) = 1/L_j(r)$, which is the time required to destroy the species j by the chemical loss reaction of interest at the given position. The advective time-scale is defined by

$$\tau_{adv}(r) = \left[\frac{1}{n_j(r)r^2}\frac{\mathrm{d}(n_j(r)r^2U_n)}{\mathrm{d}r}\right]^{-1}. \quad (12)$$

Two mechanisms are playing together: the geometric or spherical expansion and the density gradient. Indeed, one can develop the expression (12) and obtain:

$$\frac{1}{\tau_{adv}} = \left(\frac{2}{r} + \frac{\mathrm{d}\ln n_j(r)}{\mathrm{d}r}\right)U_n = \frac{2U_n}{r} - \frac{U_n}{H_j}, \quad (13)$$

where H_j is the density scaleheight of the ion species j (opposite sign with respect to the density gradient one). Due to the spherical expansion of the gas, the usual advective time-scale needs to be corrected by $2U_n/r$.

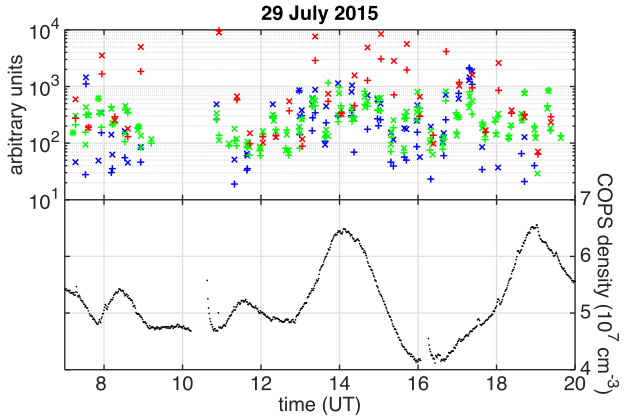

Figure 5. Plots of ion counts in log scale and arbitrary units (top panel) and uncalibrated COPS densities (bottom panel) for 2015 July 29. The colours refer to H_2O^+ (blue), H_3O^+ (red) and NH_4^+ (green), as for Fig. 2. The plus signs (+) [respectively crosses (×)] correspond to the channel A (respectively B). Statistical errors cannot be seen distinguishably in log scale. The variations of the ion number densities can be affected by the swivelling of *Rosetta*.

As illustrated by in Fig. 4 in the case of weak outgassing, the loss of H_3O^+ is always dominated by transport and not by reaction with NH_3 yielding NH_4^+. This means that NH_4^+ could not efficiently be produced by chemistry in the coma that is expected for a non- or weakly collisional coma.

Based on correlation with manoeuvres and the loss time-scales, we can conclude that NH_4^+ detected in 2015 January was not of cometary origin.

4.2 2015 July 29

Results for 2015 July 29 are shown in Fig. 5: the derived amount of H_2O^+, H_3O^+ and NH_4^+ detected signal compared to COPS local neutral density for 2015 July 29. Each ion species varies by one (H_2O^+, NH_4^+) up to two (H_3O^+) orders of magnitude. This is quite unexpected for H_2O^+: as detailed in Section 3.2, for this cometary activity, H_2O^+ is expected to be constant (∼100 cm^{-3}, see equation 8, thereafter see Fig. 7) and independent of the H_2O density. The H_2O^+ and NH_4^+ densities follow a similar trend, following the increase of COPS neutral density, with a $[NH_4^+]/[H_2O^+]$ ratio ranging from ∼0.2 to ∼6 (e.g. 12–16 UT in Fig. 5, during periods when H_2O^+ is 'trustworthy'). Moreover, the $[NH_4^+]/[H_3O^+]$ ratio, ranging from ∼0.01 to ∼3, peaked at 14 UT and 19 UT, and fell just before 16 UT, as the COPS density. However, at 19 UT, although the COPS density seemed similar than at 14 UT, the ion behaviour was not the same, in particular a lower amount of H_2O^+ at 19 UT. One should be aware that the spacecraft slewed on this day:

(i) between 11 UT and 14:30 UT, the nadir off-pointing varied between 0.2° and 0.6° with a period of ∼20 min,

(ii) between 15:30 UT and 19:30 UT, this varies between 0.4° and 1.2° with a period of ∼30 min.

As a result, the S/C slew and ion ratio may have been polluted by S/C outgassing, as attested by the large amount of H_2O^+.

To improve the confidence of our data analysis, because the MCP detector can perform two independent measurements simultaneously, one on each channel on the detector, we looked at the signal

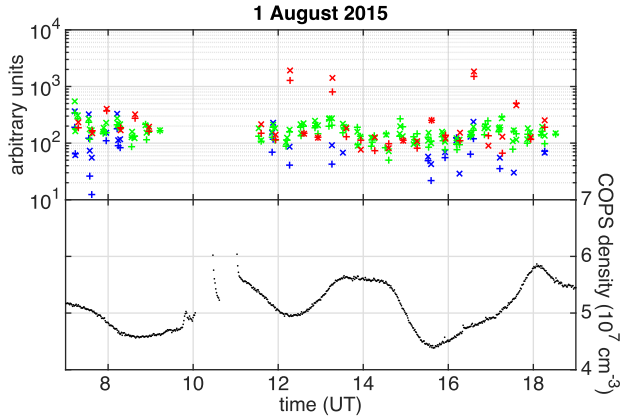

Figure 6. Same as Fig. 5 but for 2015 August 1. The Nadir off-pointing is 0.3°, except between 8 UT and 9.30 UT. The uncalibrated COPS density spikes between 10 UT and 11 UT may be relied to wheel offloading.

from both channels: one MCP channel is always slightly more sensitive by a few per cent to a few tens of percent. H_3O^+ counts show higher values (more than $\sim 10^3$ au with a factor up to 3 between both channels) than NH_4^+. The variability in H_3O^+ between both channels (up to a factor of 4) in comparison to NH_4^+ variability (factor close to 1, up to 2 once) is puzzling. In addition, H_3O^+ does not seem to follow the same trend as found for other ion species. Unfortunately, we cannot derive a rigorous quantitative ratio because of limitation in the number of samples for H_3O^+ (32 scans × 2 channels, three times less than for H_2O^+ and NH_4^+).

4.3 2015 August 1

Fig. 6 shows the results for 2015 August 1, with the same colours and ranges as in Fig. 5. The number of observations is similar to July 29 (i.e. 28 scans × channels). The number of detections of H_2O^+ is relatively low compared with NH_4^+ that belongs to the same ion mass bin: H_2O^+ is missing or below the threshold that we imposed for the analysis.

The density measured by COPS varied less on August 1 compared to July 29, ranging from 4.5×10^7 to 6×10^7 cm^{-3} compared with 4×10^7 to 6.5×10^7 cm^{-3}. This weaker variation might be correlated with the measured ion densities: the variation of each ion species during the day is much less than for July 29, the $[NH_4^+]/[H_3O^+]$ ratio ranges between 0.1 and 4. The NH_4^+ number density is higher than H_2O^+ and H_3O^+ ones. NH_4^+ is regularly higher than H_3O^+, except a few times (e.g. 12:15 UT, 13:16 UT and 16:36 UT) when H_3O^+ showed values 10 times higher than the rest of the day, up to 10^3, for both channels. However, as for July 29, the $[NH_4^+]/[H_3O^+]$ ratio peaked between 13 UT and 15 UT, and dropped around 16 UT together with the COPS density. Away from manoeuvres (between 8:15 UT and 9:15 UT), the ratio $[NH_4^+]/[H_3O^+]$ is correlated with COPS with $[NH_4^+]/[H_3O^+] > 1$ at n_n peaks, and $[NH_4^+]/[H_3O^+] < 1$ for n_n troughs.

5 COMPARISON OF DFMS ION COMPOSITION WITH THE IONOSPHERIC MODEL

In Section 5, we compare the results from our case studies (2015 July 29 and 2015 August 1) with our ionospheric model. Fig. 7 shows density profiles of each ion species for different outgassing rates Q and $[NH_3]/[H_2O]$ mixtures, for conditions close to those for 2015 August 1. We plot the density profiles of H_2O^+, H_3O^+ and NH_4^+ with/without NH_3. For a high cometary activity, NH_4^+ may be the dominant ion in the first 50 km above the surface, decreasing rapidly at higher cometocentric distances because of transport and electron recombination. As shown in Fig. 8, depending strongly on the velocity, H_3O^+ is lost by reacting with NH_3 between the surface and ∼10 km (high U_n) or ∼100 km (low U_n), yielding NH_4^+. The decrease of the NH_4^+ number density is sharper than H_3O^+ because at high cometocentric distances H_3O^+ can still be produced by the reaction between H_2O and H_2O^+, whereas NH_4^+ is produced by the reaction between NH_3 and H_3O^+ requiring one more reaction compared with H_3O^+.

In Table 1, we report results from a set of runs with different outgassing rates ($Q = 10^{27}$, 5×10^{27}, 10^{28} and 5×10^{28} s^{-1}) and volume mixing ratios of ammonia ($f_{NH_3} = 0.1$ per cent and 1 per cent). For each different initial condition of the model, we provide the ratio $[NH_4^+]/[H_3O^+]$: the red numbers correspond to most physical conditions constrained by COPS and DFMS observations (respectively for the outgassing rate and the mixing ratio) at 150 and 200 km. The ratio $[NH_4^+]/[H_2O^+]$ is not provided: although both species are found in the same spectrum, H_2O^+ was frequently close to or below our threshold. A quantitative analysis was therefore not possible. In addition, its high variability – covering more than two orders of magnitude – seems to imply contamination by spacecraft outgassing (see further discussion later in this section). For both case studies, the distance is close to 200 km and thus the expected ratio would be in the range [0.1, 0.4]. This table also shows the effect of the uncertainty in the outflow velocity: a high velocity tends to decrease the ratio $[NH_4^+]/[H_3O^+]$ by a factor of ∼2.

Given the *Rosetta* distance from the nucleus, on the one hand, NH_4^+ would be at the same or one order of magnitude less compared to H_3O^+ for July 29 (see Fig. 5). On the other hand, on August 1 (see Fig. 6), the $[NH_4^+]/[H_3O^+]$ ratio was surprisingly high (>1) and only a huge mixing ratio of NH_3, more than 1 per cent, could explain the observations, maybe caused by a heterogeneous ammonia mixing ratio on the surface. Unfortunately, the DFMS neutral composition is not available for August 1 to constrain background conditions of our simulation. Nevertheless, this $[NH_4^+]/[H_3O^+]$ ratio seems to be correlated with the COPS density for both days as predicted by the model even if its absolute value presents discrepancies.

Moreover, we would like to point out the variability of H_2O^+: according to our results, the density of H_2O^+ should be constant with respect to the distance, in photochemical equilibrium, which is not the case as it varies over several orders of magnitude. According to Fig. 8, its loss time-scale is significantly lower than the advection time by three orders of magnitude close to the surface, which means the left-hand-side term in equation (7) may be neglected and its density would be around 100 cm^{-3} (see equation 8). Discrepancies between observed and modelled H_2O^+ variability over two orders of magnitude are discussed in Section 6.3.

Finally, the possible variations of each ion number density might be correlated with the spacecraft's pointing. We checked for an eventual correlation with the nadir off-pointing angle for these days: this was stable and less than 2° that excludes such a correlation. There were still possible signatures of manoeuvres (around 6 UT or after periods without data) but they last typically tens of minutes.

6 DISCUSSION

In Section 6, we discuss the agreements and discrepancies between data and model results, and provide possible explanations.

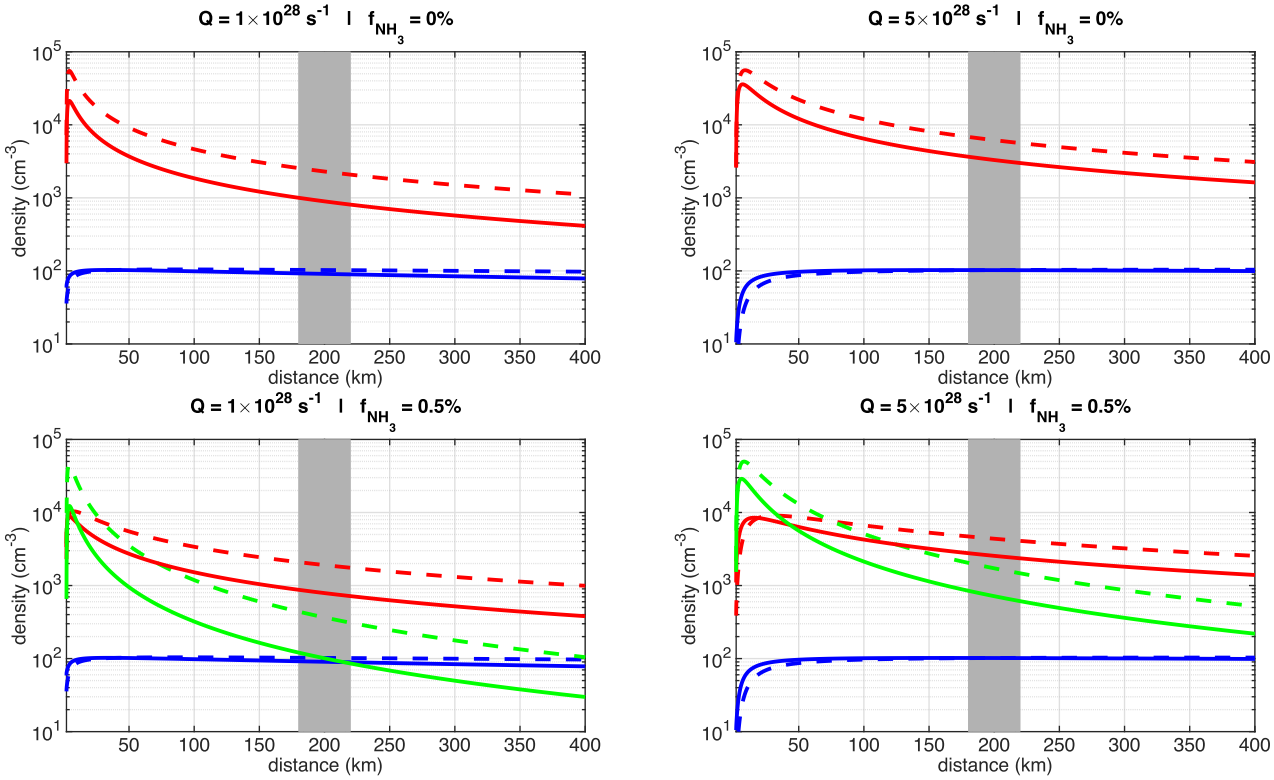

Figure 7. Plots of the modelled ion densities (H_2O^+ in blue, H_3O^+ in red, NH_4^+ in green) without ammonia (top panels) and with 0.5 per cent (bottom panels) for two different outgassing rates ($Q = 10^{28}$ s^{-1}, left panels and 5×10^{28} s^{-1}, right panels). The dotted lines refer to a neutral velocity of 500 m s^{-1}, the solid lines to 1000 m s^{-1}. As explained in Section 3.2, H_2O^+ density is close to the photochemical equilibrium (away from the surface) and thus, to a constant value. The grey area corresponds to the range for the cometocentric distance of *Rosetta* for 2015 July 29 and August 1.

Table 1. Relative proportion of NH_4^+ with respect to H_3O^+ for different outgassing rates, neutral velocity outflows and fractions of NH_3 in the coma at 150 km/200 km. The values in red correspond to the expected ones for the case studies.

Fraction of ammonia f_{NH_3} in the coma	U_n (m s^{-1})	Q (molecules s^{-1})			
		1×10^{27}	5×10^{27}	1×10^{28}	5×10^{28}
		150 km/200 km	150 km/200 km	150 km/200 km	150 km/200 km
0.1 per cent	500	1.9 per cent/1.5 per cent	4.2/3.3 per cent	5.5/4.3 per cent	11.0/8.4 per cent
	1000	0.8/0.7 per cent	2.4/2.0 per cent	3.7/3.0 per cent	8.3/6.5 per cent
0.5 per cent	500	8.4/6.9 per cent	18.0/14.4 per cent	24.4/19.2 per cent	51.2/39.4 per cent
	1000	3.7/3.2 per cent	10.5/8.8 per cent	15.6/12.8 per cent	35.3/28.0 per cent
1 per cent	500	15.4/12.8 per cent	33.3/26.7 per cent	45.7/36.1 per cent	99.2/76.3 per cent
	1000	7.1/6.1 per cent	19.2/16.0 per cent	28.3/23.2 per cent	65.3/51.9 per cent

6.1 Model assumptions

The model is based on the solution of a set of continuity equations and thus a fluid approach. As mentioned by Mandt et al. (2016), the ion exobase is only a few hundred kilometres above the surface (beyond 400 km for our observation periods). This limit defines the transition between the fluid and kinetic regimes for ions in the coma:

(i) between the surface and the ion exobase: collisions are sufficient to thermalize ions with neutrals
(ii) above the ion exobase: collisions are too scarce to sufficiently thermalize the ions with the rest of the cometary species.

For these days, *Rosetta* was at 200 km, in the inner region i.e. below the ion exobase or collisionopause around 400 km. This means the dynamic/motion of ions is still dominated by the collisions with neutrals and not by external forces/accelerations (e.g. pick-up process). As a result, treating the ions as a fluid (and thus using the continuity equation) is suitable up to this bound. Moreover, the detection of cometary NH_4^+ ions attests to the lack of acceleration of the ion population (see Section 6.2), which allows to have ion chemistry occurring in the coma.

Regarding the neutral composition, a mixture of pure water and ammonia is assumed in the model. Other minor species were not considered. CO_2 and CO were investigated in this work but they do not play a key-role in the photochemistry of NH_4^+, so that they are not considered for these simulations presented. However, other minor species, like H_2S, H_2CO, HCN, HCOOH, CH_3OH, HCNO, HNC, will be the topic of future investigation. Indeed, these species have intermediate proton affinities, between H_2O and NH_3 (Hunter & Lias 1998; Vigren & Galand 2013). NH_4^+ still remains the terminal

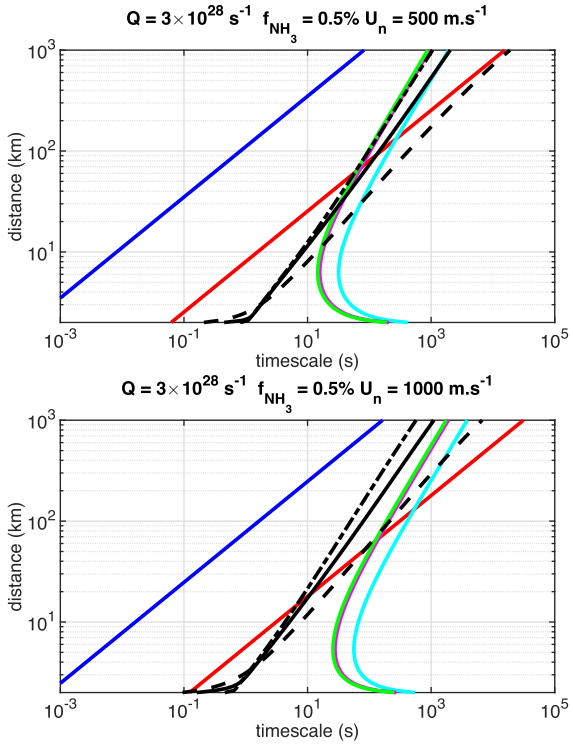

Figure 8. Loss time-scales for H_2O^+, H_3O^+ and NH_4^+ for $U_n = 500$ (top panel) and 1000 m s^{-1} (bottom panel) for $Q = 3 \times 10^{28}$ s^{-1} and $f_{NH_3} = 0.5$ per cent, similar to 2015 August. Please refer to Fig. 4 for the description.

Table 2. List of species detected within the coma of 67P/C-G (except HNC that is undistinguishable from HCN, Le Roy et al. 2015) with intermediate proton affinities. The colours correspond to the neutral species of which the protonated forms are investigated in this paper i.e. H_2O^+ (blue), H_3O^+ (red) and NH_4^+ (green). The values are from Hunter & Lias (1998).

Species	Proton affinity (eV)
HO	6.16
H_2O	7.17
H_2S	7.32
H_2CO, HCN	7.40
HCOOH	7.70
CH_3OH	7.83
HCNO	7.87
HNC	8.02
NH_3	8.86

ion for the proton exchange reaction, but these species could still participate in the destruction of H_3O^+ and to the production of NH_4^+ and therefore affect the $[NH_4^+]/[H_3O^+]$ ratio:

$$\begin{cases} H_3O^+ + M \rightarrow H_2O + MH^+ \\ NH_3 + MH^+ \rightarrow NH_4^+ + M, \end{cases} \quad (14)$$

where M is a species with an intermediate proton affinity (cf. Table 2).

Additional assumptions could also be reviewed in the future. The electron temperature, which drives the electron–ion dissociative recombination rates, has here been assumed to be constant at 200 K. This value is expected to represent a lower limit in the light of the Rosetta Plasma Consortium (RPC) - Langmuir Probe (LAP) measurements, at least at the location of *Rosetta* (Odelstad et al. 2015). This also implies that the ion–electron recombination rates are upper limits in this paper and the losses are overestimated. A sensitivity study of the ionospheric densities with T_e was undertaken by Vigren & Galand (2013): the total ionospheric number density varies by a factor of 2 or more for T_e varying between 10 and 1000 K. In order to assess the sensitivity of ion composition with T_e, we have ran the ionospheric model for $T_n = T_i = T_e = 50$ K and for $T_n = T_i = 200$ K and $T_e = 1000$ K. For $T_n = T_i = T_e = 50$ K, the NH_4^+ to H_3O^+ number density ratio changes at 150 km/200 km from 51.2 per cent/39.4 per cent (200 K) to 64.4 per cent/49.4 per cent (50 K), for $U_n = 500$ m s^{-1} and $Q = 5 \times 10^{28}$ s^{-1}. For $T_n = T_i = 200$ K and $T_e = 1000$ K, this ratio changes to 66.1 per cent/56.1 per cent under the same Q and U_n. Furthermore, the photodissociation of cometary neutrals producing minor species is not included. The photoelectron impact ionization is neglected here, as the coma of 67P is too thin for efficient soft X-rays absorption and to allow significant production of energetic photoelectrons (see Vigren & Galand 2013, Fig. 6). This was, however, not the case for comet 1P/Halley (Haider & Bhardwaj 2005), or for high outgassing comets in general (Bhardwaj 2003).

Finally, we have investigated the sensitivity of our model that is based on the assumption of an isothermal coma. For the period of interest, we ran a simulation assuming isentropic outflow of the gas with the associated cooling due to the gas expansion. For $n_n = 2.5 \times 10^7$ cm^{-3} at 180 km (conditions that correspond to the case of $Q = 1 \times 10^{28}$ s^{-1} and $U_n = 1000$ m s^{-1} in Table 1, $f_{NH_3} = 0.5$ per cent and $U_n(180\,\text{km}) \sim 950$ m s^{-1}), the $[NH_4^+]/[H_3O^+]$ ratio is 13.3 per cent/10.5 per cent (150 km/200 km) to be compared with 15.6 per cent/12.8 per cent in Table 1.

6.2 Solar wind comet interaction

Comet 67P/C-G is surrounded by the solar wind and its interaction is very dynamic: the activity of 67P/C-G is relatively low compared with 1P/Halley and thus, the different and well-defined boundaries observed at 1P do not appear clearly and/or were not at 67P/C-G.

As detailed by Balsiger et al. (1986) and Neubauer et al. (1986), Giotto crossed a well-defined boundary at ∼4600 km from 1P/Halley, the so-called contact surface. Inside the contact surface, the most dominant ionization process is photoionization (Allen et al. 1987). For 67P/C-G, first reports near perihelion of RPC/MAG observations reveal that the diamagnetic cavity is much closer to the surface (around ∼170–300 km, Goetz et al. 2016), though farther away than model predictions (Benna & Mahaffy 2006; Hansen et al. 2007; Koenders et al. 2015). The nearness of this boundary, similar to the non-trivial relation between the plasma and the neutral gas requires some caution to the assumption of a radial coupled outflow of ions and neutrals in our model.

In addition, the direct interaction between the solar wind and cometary ions is not well understood. Indeed, as the Solar wind plasma is propagating with the velocity vector $\boldsymbol{v}_{SW}$ through a magnetic field $\boldsymbol{B}$, this generates the so-called motional or convective electric field $\boldsymbol{E}_{conv} = -\langle \boldsymbol{v} \rangle \times \boldsymbol{B}$, with $\langle \boldsymbol{v} \rangle$ the mean ion outflow (combination of cometary and solar wind ions), affects the newborn cometary ions. As H_2O^+, H_3O^+ and NH_4^+ have close masses, one could expect these ions to experience similar accelerations and thus have similar behaviours in their detection but this also depends on which distance from the surface they are mainly produced, which is different for each of these species.

Nevertheless, one outcome of our study is that, during the period analysed, the detection of NH_4^+ suggests that no strong acceleration of ions would prevent its production. This is consistent with the fact that *Rosetta* was below the ion exobase, where collisions with ions may still occur.

6.3 H_2O^+ variability

As mentioned earlier in Section 5, we looked at H_2O^+ variability because the model predicted a constant density. Large variations in H_2O^+ were observed, especially on July 29 (see Fig. 5).

First, the spacecraft is a source of water, both neutral and ionized, through outgassing of gas frozen on its surfaces. After manoeuvres, sharp peaks in H_2O – as seen in COPS – and increases in H_2O^+ are observed (e.g. 17:17 UT on July 29 in Fig. 5).

Secondly, the DFMS observations should be linked to the DFMS field of view in ion mode (Schläppi 2011): by sampling a small fraction of the velocity space, the detection of ions is highly sensitive to anisotropic process governing the ion dynamics.

The ion behaviour and motion in the vicinity of the comet (e.g. within the diamagnetic cavity) and *Rosetta* (e.g. the spacecraft potential) needs further investigations

7 CONCLUSION

Using the mass spectrometer ROSINA/DFMS on-board *Rosetta*, it has been possible to unambiguously detect NH_4^+ of cometary origin for the first time. Thanks to its high spectral resolution ion mode, this instrument is able to distinguish NH_4^+ from H_2O^+, which was not possible at comet 1P/Halley due to the limited mass resolution of the Giotto IMS instrument (Balsiger et al. 1987). As predicted by Vigren & Galand (2013), and confirmed here by ionospheric modelling adjusted to the conditions encountered, near perihelion the cometary activity was enough to efficiently trigger the production of NH_4^+ in the coma of 67P/C-G and to enable its detection close to the comet at 200 km. The detection of NH_4^+, and in comparable abundances with H_3O^+, brings evidence of an extended region of efficient ion–neutral chemistry not hampered by ion acceleration, in consistency with the fact that *Rosetta* was below the estimated location of the ion exobase during the period of observations. It is, however, difficult from the present data to completely rule out more complex ion trajectories influenced by both magnetic and electric fields, which would tend to affect the trajectories of the considered ion species in roughly similar ways due to their nearly similar mass-to-charge ratios.

The results from our ionospheric model are consistent with the DFMS observations and the presence of NH_4^+ near perihelion. Our first analysis is promising and planned refinements of our model are expected to further improve the match to the ion composition data obtained at 67P/C-G, such as:

(i) the addition of intermediate proton affinity species,

(ii) the addition of hydrocarbons, such as CH_4, undergoing photoionization,

(iii) the chemistry of minor and parent neutral species, such as NH_3, which can undergo photodissociation, yielding NH and NH_2, followed by photoionization.

ACKNOWLEDGEMENTS

Work at Imperial College London is supported by STFC of UK under grants ST/K001051/1 and ST/N000692/1. Work on ROSINA at the University of Bern was funded by the State of Bern, the Swiss National Science Foundation and the ESA PRODEX Program. Work at BIRA-IASB was supported by the Belgian Science Policy Office via PRODEX/ROSINA PEA90020 and 4000107705 and by the F.R.S.-FNRS grant PDR T.1073.14 'Comparative study of atmospheric erosion'. We are indebted to the ROSINA operation and data processing teams. We acknowledge the staff of CDDP and Imperial College London for the use of AMDA and the RPC Quicklook data base (provided by a collaboration between the Centre de Données de la Physique des Plasmas, supported by CNRS, CNES, Observatoire de Paris and Université Paul Sabatier, Toulouse and Imperial College London, supported by the UK Science and Technology Facilities Council). Work at Swedish Institute of Space Physics is supported by the Swedish National Space Board (166/14). Work at Southwest Research Institute is supported with contract through the Jet Propulsion Laboratory.

REFERENCES

Allen M., Delitsky M., Huntress W., Yung Y., Ip W.-H., 1987, A&A, 187, 502
Altwegg K. et al., 1993, A&A, 279, 260
Balsiger H. et al., 1986, Nature, 321, 330
Balsiger H. et al., 1987, J. Phys. E: Sci. Instrum., 20, 759
Balsiger H. et al., 2007, Space Sci. Rev., 128, 745
Benna M., Mahaffy P. R., 2006, Geophys. Res. Lett., 33, L10103
Bhardwaj A., 2003, Geophys. Res. Lett., 30, 2244
Bieler A. et al., 2015, Nature, 526, 678
Bird M. K., Janardhan P., Wilson T. L., Huchtmeier W. K., Gensheimer P., Lemme C., 1997, Earth Moon Planets, 78, 21
Biver N. et al., 2015, European Planetary Science Congress 2015. Available at: http://meetingorganizer.copernicus.org/EPSC2015
Bockelee-Morvan D., 1997, in van Dishoeck E. F., ed., IAU Symp. Vol. 178, Cometary volatiles: The status after comet C/1996 B2 Hyakutake. Cambridge Univ. Press, Cambridge, p. 219
Churyumov K. I., Gerasimenko S. I., 1972, in Chebotarev G. A., Kazimirchak-Polonskaia E. I., Marsden B. G., eds, IAU Symp. Vol. 45, The Motion, Evolution of Orbits, and Origin of Comets. Int. Astron. Union, Dordrecht, Reidel, p. 27
De Keyser J. et al., 2015, Int. J. Mass Spectrom., 393, 41
Dello Russo N., Vervack R. J., Weaver H. A., Biver N., Bockelée-Morvan D., Crovisier J., Lisse C. M., 2007, Nature, 448, 172
Dello Russo N., Vervack R. J., Weaver H. A., Kawakita H., Kobayashi H., Biver N., Bockelée-Morvan D., Crovisier J., 2009, ApJ, 703, 187
Dello Russo N. et al., 2011, ApJ, 734, L8
Fuselier S. A. et al., 2015, A&A, 583, A2
Fuselier S. A. et al., 2016, MNRAS, 462, S67
Goetz C. et al., 2016, A&A, 588, A24
Haider S., Bhardwaj A., 2005, Icarus, 177, 196
Haider S., Bhardwaj A., Singhal R., 1993, Icarus, 101, 234
Hanner M. et al., 1985, Icarus, 64, 11
Hansen K. C. et al., 2007, Space Sci. Rev., 128, 133
Hässig M. et al., 2015, Science, 347, 6220
Hunter E. P. L., Lias S. G., 1998, J. Phys. Chem. Ref. Data, 27, 413
Kawakita H. et al., 2013, Icarus, 222, 723
Koenders C., Glassmeier K.-H., Richter I., Ranocha H., Motschmann U., 2015, Planet. Space Sci., 105, 101
Lamy P. L., Toth I., Davidsson B. J. R., Groussin O., Gutiérrez P., Jorda L., Kaasalainen M., Lowry S. C., 2007, Space Sci. Rev., 128, 23
Le Roy L. et al., 2015, A&A, 583, A1
Mandt K. E. et al., 2016, MNRAS, 462, S9
Meier R., Eberhardt P., Krankowsky D., Hodges R. R., 1994, A&A, 287, 268
Mumma M. J. et al., 2011, ApJ, 734, L7
Neubauer F. M. et al., 1986, Nature, 321, 352
Odelstad E. et al., 2015, Geophys. Res. Lett., 42, 10126

Paganini L. et al., 2014, AJ, 147, 15
Palmer P., Wootten A., Butler B., Bockelee-Morvan D., Crovisier J., Despois D., Yeomans D. K., 1996, BAAS, 28, 927
Rubin M., Hansen K. C., Gombosi T. I., Combi M. R., Altwegg K., Balsiger H., 2009, Icarus, 199, 505
Rubin M., Tenishev V. M., Combi M. R., Hansen K. C., Gombosi T. I., Altwegg K., Balsiger H., 2011, Icarus, 213, 655
Schläppi B., 2011, PhD thesis, Univ. Bern
Schläppi B. et al., 2010, J. Geophys. Res., 115, A12
Tenishev V., Combi M., Davidsson B., 2008, ApJ, 685, 659
Vigren E., Galand M., 2013, ApJ, 772, 33
Wegmann R., Schmidt H. U., Huebner W. F., Boice D. C., 1987, A&A, 187, 339

APPENDIX: COMPUTATION OF THE VOIGT PROFILE

We favour the fitting of DFMS data by one Voigt profile and not by a double Gaussian. Although both were tested and provided comparable results (i.e. similar residuals), the Voigt profile requires one parameter less than two Gaussians. Indeed, the VD requires one centre, one amplitude and two standard deviations whereas the two-Gaussian distribution needs one centre, two different standard deviations and two amplitudes.

One difficulty is that the Voigt normalized distribution $V(x, \sigma, \gamma)$ does not have an analytical expression and is defined by the convolution between a Gaussian distribution and a Lorentzian distribution, given by:

$$V(x, \sigma, \gamma) = \int_{-\infty}^{+\infty} \frac{\gamma}{\sigma\sqrt{2\pi^3}} \frac{1}{(x-t)^2 + \gamma^2} \exp\left(-\frac{t^2}{2\sigma^2}\right) \mathrm{d}t, \tag{A1}$$

where σ^2 and γ^2 are the variances of the Gaussian and the Lorentzian distributions, respectively. As the convolution of two normalized distributions, the VD has the following property:

$$\int_{-\infty}^{+\infty} V(x, \sigma, \gamma)\, \mathrm{d}x = 1. \tag{A2}$$

A priori, it would not be easy to compute/evaluate numerically such an integral with a sufficient accuracy. However, one can see that the form of the integral A1 is the one required for applying the Gauss–Hermite quadrature, i.e.

$$\int_{-\infty}^{+\infty} \exp(-x^2) f(x)\, \mathrm{d}x \approx \sum_{i=1}^{n} W_{i,n} f(X_{i,n}), \tag{A3}$$

where X_i ($i = 1, 2, .., n$) are the roots of the Hermite polynomial H_n of degree n and W_i are the associated weights defined as

$$W_{i,n} = \frac{2^{n-1} n! \sqrt{\pi}}{n^2 H_{n-1}^2(X_{i,n})}. \tag{A4}$$

After some transformations, one obtains for the approximated VD:

$$V(x, \sigma, \gamma) \approx \frac{\gamma}{\pi\sqrt{\pi}} \sum_{i=1}^{n} \frac{W_{i,n}}{(\sqrt{2}\sigma X_{i,n} + x)^2 + \gamma^2}. \tag{A5}$$

The choice of n should be sufficiently high but not be necessarily too high (typically $\leq$100) because of the machine precision and computational requirements: $W_{i,n}$ decreases quickly to 0 for increasing i (for example, $W_{100,100} \approx 5.9 \times 10^{-79}$) and thus does not contribute to the sum.

This paper has been typeset from a TEX/LATEX file prepared by the author.